Experimental Analysis of a Scaled-Down Vestas Four-Rotor Wind Turbine

Experimental Analysis of a Scaled-Down Vestas Four-Rotor Wind Turbine

Oliver Tierdad Filsoof[1,2], Anders Yde[2], Peter Bøttcher[2], Xuping Zhang[1]

[1] Department of Engineering, Inge Lehmanns Gade 10, Aarhus, Denmark
[2] Vestas Wind System A/S, Hedeager 42, Aarhus, Denmark

E-mail: otf@eng.au.dk, xuzh@eng.au.dk

Abstract. In this work, a 1/30 scaled-down Vestas four-rotor demonstrator wind turbine is established as an experimental setup. The experimental setup is used to analyze how the structural natural frequencies are affected by the rotor speed for a multi-rotor wind turbine. To have comparable dynamic behavior between the Vestas turbine and the experimental setup, Froude scaling is used. For standstill tests, a metal brushing technique is employed to excite the setup, and when rotating an automated impulse mechanism provide impulses to the rotor blades. Modal testing experiments are conducted, and testing results show that standstill frequencies between the Vestas turbine and experimental setup coincided. The experiment demonstrates that by using the automated impulse mechanism from 40 rpm to 110 rpm, edgewise whirling modes are excited and proportional to the rotor speed. The setup experiences large vibrations if the rotor speed continues increasing beyond 110 rpm using the impulse mechanism. Switching to the metal brushing technique achieves better results, and makes it possible to see that both the flapwise and edgewise whirling modes are proportional to the rotor speed.

1. Introduction

The need for renewable energy sources to replace fossil fuel has never been more urgent than it is today because of climate changes. One of the most promising renewable energy sources is wind energy which can be converted to electricity using wind turbines. A conventional wind turbine consists of a tower and a three-bladed rotor to harvest the kinetic energy from the wind. To lower the Levelized Cost of Energy, the trend is to increase the rotor size. The reason for this is that it increases the capacity factor of the wind turbine. However, the downside is that large blades are expensive, difficult to transport, and complicated to manufacture. Instead of increasing the rotor size to get a larger power output, a multi-rotor wind turbine (MRWT) becomes the alternative of thinking. The idea of a MRWT is to split the rotor area into n smaller areas. MRWT designs have been conducted, and in 2016 Vestas erected a four-rotor concept demonstrator wind turbine, which is illustrated in Figure 1. The tip height was 75 m, and it had four 225 kW rotors providing a 900 kW power output in total. The blade radius was 14.5 m, but to generate a 900 kW using a single-rotor wind turbine (SRWT), the blade length needs to be doubled [1]. As it is seen in Figure 1, the structure supporting the rotors increases the complexity of its dynamic behavior.

The dynamic behavior of SRWTs have been in interest for researchers in many years [2, 3, 4, 5, 6] while this is not the case for MRWTs. Recent studies by Filsoof et al [7] investigated

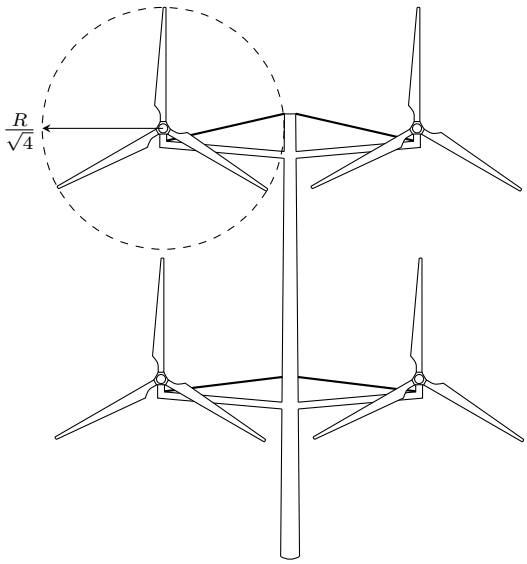

Figure 1. Illustration of Vestas four-rotor concept demonstrator. Tip height was 75 m, and it had four 27 m rotors. R refers to the radius for a single-rotor wind turbine with the equivalent power output.

the modal dynamics of MRWTs analytically by first linearizing the equations of motions at an equilibrium point and then applying the Coleman transformation matrix to each rotor to make the system time-invariant. These results were later used to establish a high-fidelity linear MRWT model by combining the aeroelastic tools HAWC2 and HAWCStab2 [8]. But the effort of experimental verification of the MRWTs dynamics is very limited [9].

This paper, therefore, aims to extend our previous efforts on experimental studies of MRWT by analyzing the modal dynamics of a scaled Vestas MRWT. To properly capture the dynamic response of the Vestas MRWT in a scaled setup, Froude scaling is used. The scaling of the Vestas MRWT and a description of the experimental setup are given in section two including excitation strategies. To analyze how frequencies change with rotor speed (Campbell diagram), the rotors on the experimental setup are set to a fixed rotor speed and exited for a period of time while accelerations are measured using accelerometers. In section three the data from the accelerometers is analyzed in frequency-domain and visualized in a waterfall plot. The last section gives the conclusion of the paper.

2. Experimental Setup

The experimental setup is for pure structural validation, which makes Froude scaling theory an appropriate method to scale-down the Vestas MRWT. The reason for this is that Froude scaling makes sure that the dynamic properties from the Vestas MRWT is properly conserved in a scaled experimental model by keeping the ratio between gravity and inertia loads constant [10]. The various scaling factors used are given in Table 1, where λ is the scaling parameter [11]. For the experimental setup $\lambda = \frac{1}{30}$ is chosen so that the tip height equal 2.5 m. The setup is illustrated in Figure 2. It consists of a tower, four arm-structures, and four-rotor systems. The tower and arm-structure are made out of circular aluminum tubes. The tower is fixed to a granite block which has good damping properties. Each arm-structure has a three-bladed rotor attached that is driven by a DC-motor, where the rotational speed is controlled by varying the input voltage. The required rotor speed for the DC-motor is found by taking the rated speed for the Vestas MRWT at 40 rpm and multiply it by the corresponding scaling factor given in

Table 1. Scaling factors between full scale model and experimental setup. λ is the scaling parameter and given as the length ratio between the scaled and full size model.

Parameter	Scaling law
Length	λ
Time	$\sqrt{\lambda}$
Rotor speed	$1/\sqrt{\lambda}$
Mass	λ^3
Moment of inertia	λ^4
Bending stiffness	λ^5

Table 1. This gives $\approx$ 220 rpm, but for better visualization of the gyroscopic forces and stress stiffening effects on the natural frequencies, the maximum speed for the motors is chosen to 250 rpm.

The rotor blades are made of rectangular aluminum profiles to imitate the different stiffness properties in the flap and edge directions. A total of 12 single-axis accelerometers of the type Brüel and Kjær 4508B are attached to the experimental setup in the ground-fixed frame of reference. This includes four at the tower to capture the first and second fore-aft tower modes, and two at the rear of each rotor to capture various arm-bending and rotor blade modes. The reason that the accelerometers have an off-set from the arm-structure is that the reaction forces from the flapwise rotor modes rotate the tip of the arm-structure in torsion and yaw. The off-set, therefore, works as an "amplifier" of these rotations.

2.1. Excitation

The excitation strategy used for this setup is based on experience from [10] where they validated numerical simulations experimentally for both a two and three-bladed SRWT. In the paper, they were able to excite both blade and tower modes by manually applying impulses to the blades at standstill and when rotating. For the experimental setup in this paper, it is difficult to adapt the manual impulse technique. Instead, an automated impulse setup is devolved, which is shown in Figure 3. The principle of this setup is, that at a fixed point in the rotor plane the blades are hitting a rigid beam with a torsional spring fixture. As the blade collide the rigid beam it transfers some of the rotors angular momentum to accelerate the beam resulting in an impulse force on the blade. The spring fixture makes sure that the beam collide with the next blade. The parameters of the mechanism, e.g. torsional spring constant, damping properties, and beam type, have been tuned manually until it transferred a sufficient impulse to the blade.

A drawback with the automated impulse mechanism is that it requires the motors to be active so that it is not possible to use for the standstill case. Instead, the experimental setup is in this case excited by manually brushing the structure using a steel brush at various locations for 5 min. This type of excitation gives a white-noise like input to the system [12].

2.2. Data Acquisition System

The data acquisition system for the the experimental setup is shown in Figure 4. The power supply provides a fixed DC voltage to the DC-motors, which leads to the fixed constant rotational speed. The rotational speed of the DC-motor is measured using an build-in encoder which is converted to RPM using a Arduino Uno. The analog output from the accelerometers is converted to a digital input for the PC using a cDAQ.

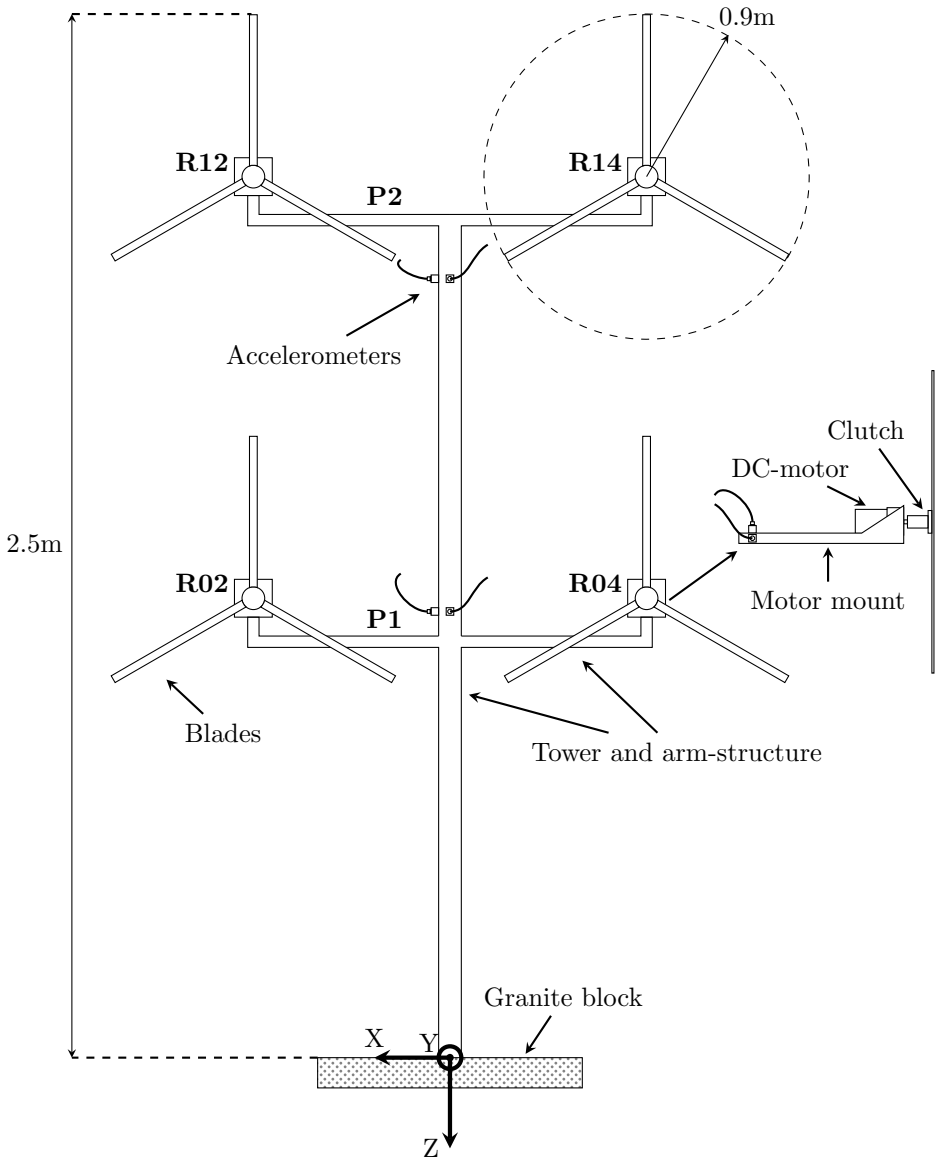

Figure 2. Illustration of the main components of the scaled experimental setup of the Vestas four-rotor wind turbine. R02, R04, R12 and R14 refers to the different rotors. P1 refers to the lower platform, and P2 to the upper platform.

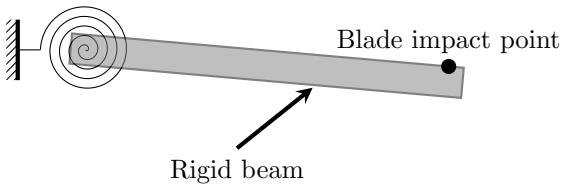

Figure 3. Automated blade impact mechanism used to excite blade modes.

2.3. Test Procedure and Post-Processing of Acceleration Data
To get an overview of how the modal frequencies of the experimental setup change as a function of rotor speed, a range of tests at fixed rotor speed are performed. First, all rotors are fixed to

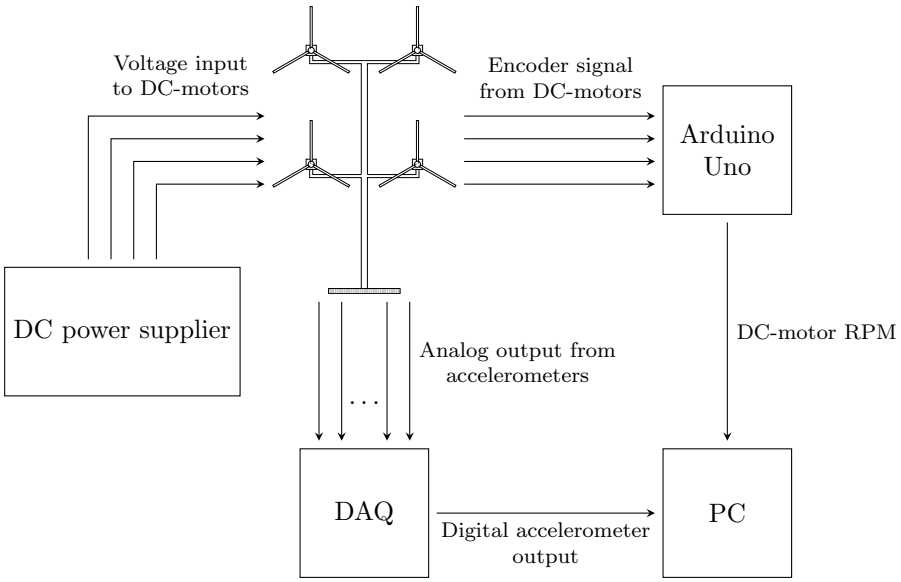

Figure 4. Flowchart of the data acquisition system.

rotate at the same speed. After this, the automated impulse mechanism is applied to excite the setup for 5 min.

The acceleration data for each fixed rotor speed is divided into 20 segments with 50 % overlap. A Hamming window is applied to each segment before being transferred into frequency-domain by discrete Fourier transformation. Taking the squared absolute value gives the power spectral density (PSD), and the segments are then averaged to filter out noise from the data. Doing this for each rotor speed, it is possible to visualize the data in a waterfall to analyze how the natural frequencies changes with the rotor speed.

3. Results and Discussion

Table 2 shows the standstill frequencies for the Vestas MRWT, experimental setup and a numerical model of the experimental setup. The numerical model is made in the aeroelastic multi-body tool HAWC2 [13]. In HAWC2 each body is discretized into several 12 degree-of-freedom linear Timoshenko beam elements. A body is assigned its own local coordinates system, and the total system is assembled in the global frame using nonlinear algebraic constraint equations. Natural frequencies are extracted in HAWC2 by direct eigenvalue analysis. The mode description is from visual inspection of the modes shapes from the numerical models of the experimental setup and Vestas MRWT. The natural frequencies for the experimental setup are found by peak picking from PSD plots. Examples of those are seen in Figure 5 for two accelerometers located at the tower top and Figure 6 for two accelerometers mounted at rotor R02. Note that the natural frequencies in each case are normalized with respect to the first edgewise blade natural frequency. This gives a better overview for comparing frequencies.

As expected, the standstill frequencies for the numerical model and experimental setup coincide. There are generally good agreements between the Vestas MRWT and experimental setup, although some of natural frequencies have significant deviations. The modes related to platform roll are 50% off in frequency, due to difficulties in making a simplified model of the interface between arms and tower. The same can be explained for the second tower side-side and fore-aft which involves tilt and roll of the platform interfaces.

Figure 5 shows the fore-aft and side-side accelerations for the lower platform (P1). The small difference in natural frequency between the first side-side and fore-aft tower mode is also seen

Table 2. Selected normalized standstill natural frequencies for the Vestas multi-rotor wind turbine (MRWT), scaled numerical model and experimental setup. The natural frequencies are normalized with respect to the first blade edgewise natural frequency. P1 refers to the lower platform and P2 to the upper platform. $(\bullet)^*$ refers to that no test have been done.

Normalized Standstill Natural Frequencies			
Mode description	Numerical model	Experiment	Vestas MRWT
1^{st} tower side-side	0.082	0.082	0.086
1^{st} tower fore-aft	0.084	0.086	0.093
1^{st} tower torsion	0.173	0.168	0.141
Asymmetric platform roll (P1,P2)	0.260	0.263	0.189
Symmetric fore-aft arm-bending (P1)	0.266	0.273	0.286
Symmetric platform roll (P1,P2)	0.309	0.300	0.212
1^{st} tower fore-aft with static rotors	0.451	0.453	-
2^{nd} tower side-side	0.570	0.630	0.626
2^{nd} tower fore-aft	1.006	-	0.828
1^{st} blade flapwise bending	0.750	0.750*	0.642
1^{st} blade edgewise bending	1	1*	1

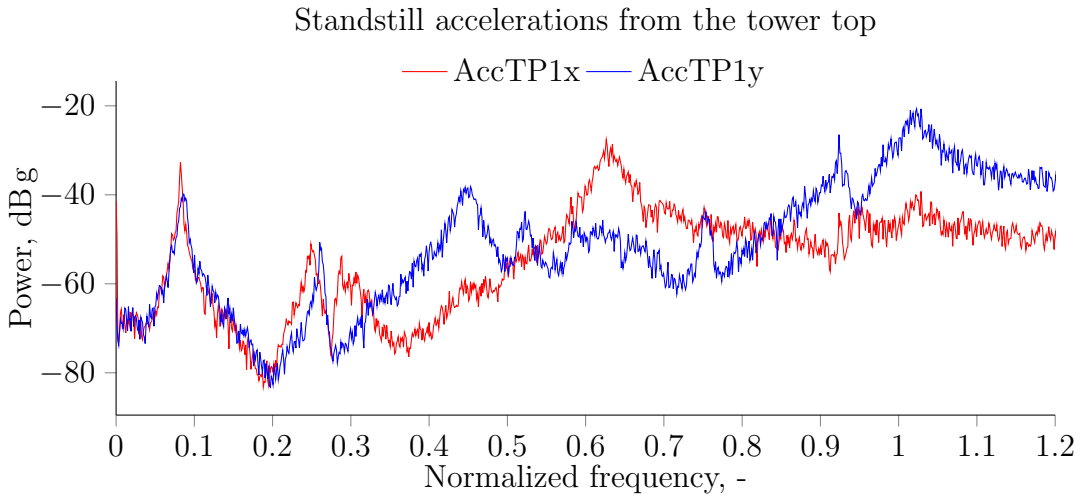

Figure 5. Power spectral density plot from standstill analysis from the two accelerometers on the tower top.

in the measurements. The accelerometers cannot capture the first torsional mode because they are mounted at the axis of rotation. Instead, this peak is captured by the accelerometers on the rotor mounts, and seen as the sharp peak at 0.168 in Figure 6. The energy concentrations at the band $0.2 - 0.35$ include various combinations of arm-bending modes and at 0.453 is the fore-aft tower mode where the tower moves fore-aft while the rotors have almost no movement. The second tower side-side mode is seen at 0.626 and the second tower fore-aft mode is close to the blade edgewise natural frequency at 1.

Rotor modes at standstill involve yaw, torsion and fore-aft movement of the arm-tip for

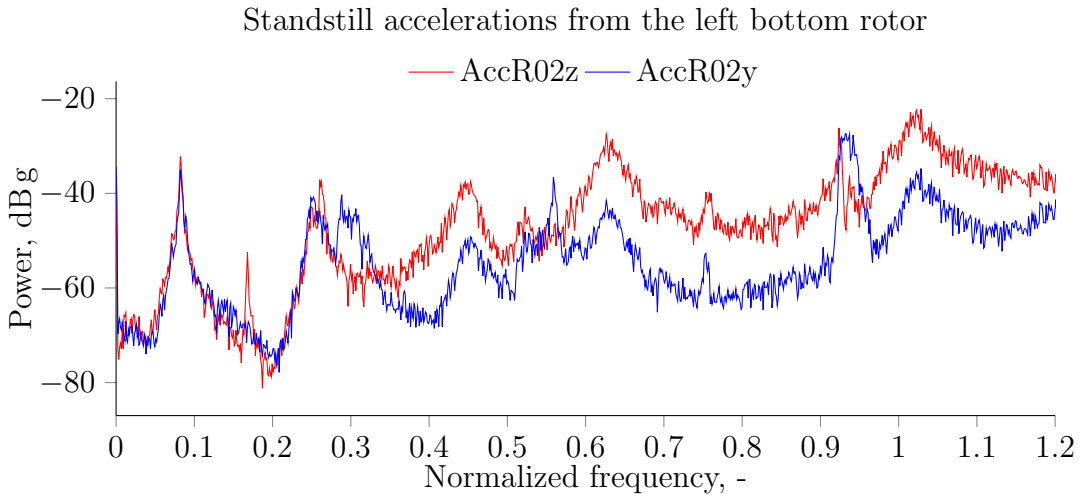

Figure 6. Power spectral density plot based on acceleration data from nacelle R02 at standstill.

flapwise rotor modes, and in-plane translations and drive-train torsion for the edgewise rotor modes [14]. The first blade flapwise and edgewise natural frequencies are given in the two last rows in Table 2. The relation between the two natural frequencies for the experimental setup differs from the Vestas MRWT but this is not considered critical. The flapwise modes which couples to arm torsion show-up in the numerical model at 0.62. Looking at Figure 5 there is also energy concentrated around that specific frequency, but only with one dominating peak, which properly is the second tower side-side mode as already mentioned. The peak at 0.75 is related to the flapwise symmetric modes by looking at the numerical model, and by noticing that the peak also is present in Figure 5 for the PSD measuring fore-aft accelerations of the tower. The peak slightly below 0.62 is not present in the numerical model, while the peak at 0.95 is the vertical edgewise mode.

Figure 7 shows a Campbell diagram to visualize natural frequencies as function of rotor speed for the accelerometer on rotor R02 oriented in the global z direction. Figure 7 (a) shows the diagram using the automated impulse mechanism, and Figure 7 (b) is based on metal brushing technique. The impulse mechanism requires the rotors to build up kinetic energy, which is the reason for that the Campbell diagram starts at 40 rpm. At 110 rpm the system experienced large vibrations so that it was not possible to increase the rotor speed any further. No problems were encountered using the metal brushing technique. Based on the results in [7, 8] it is expected that the edgewise and flapwise modes split with $-\Omega$ for backward whirling, and $+\Omega$ for the forward whirling when the rotor speeds are the same for a MRWT. This is confirmed and seen in both Campbell diagrams around the edgewise natural frequency, but only in Figure 7 (b) for the flapwise natural frequency. Both frequency splits have quite a wide band, compared to the first fore-aft/side-side tower mode. The reason for this is that increasing the number of rotors increases the number of backward and forward whirling modes. As an example, the flapwise mode resulting in a yaw movement at the arm-tip couples to the flapwise backward whirling mode at rotation. The four rotors leads to four combinations of this mode (rotor symmetric and asymmetric). The natural frequencies of these modes are slightly different due to how their reactions force effects the tower and arms. Another aspect that results in the broad frequency band is that the rotors are not perfectly isotropic and can differ in both mass and stiffness.

The frequency splitting for both the flapwise and edgewise modes occur slightly lower than predicted by the numerical model. The reason for this can properly be found in that there is some play from the DC-motor shaft to the rotor blades, which is not taken into account in

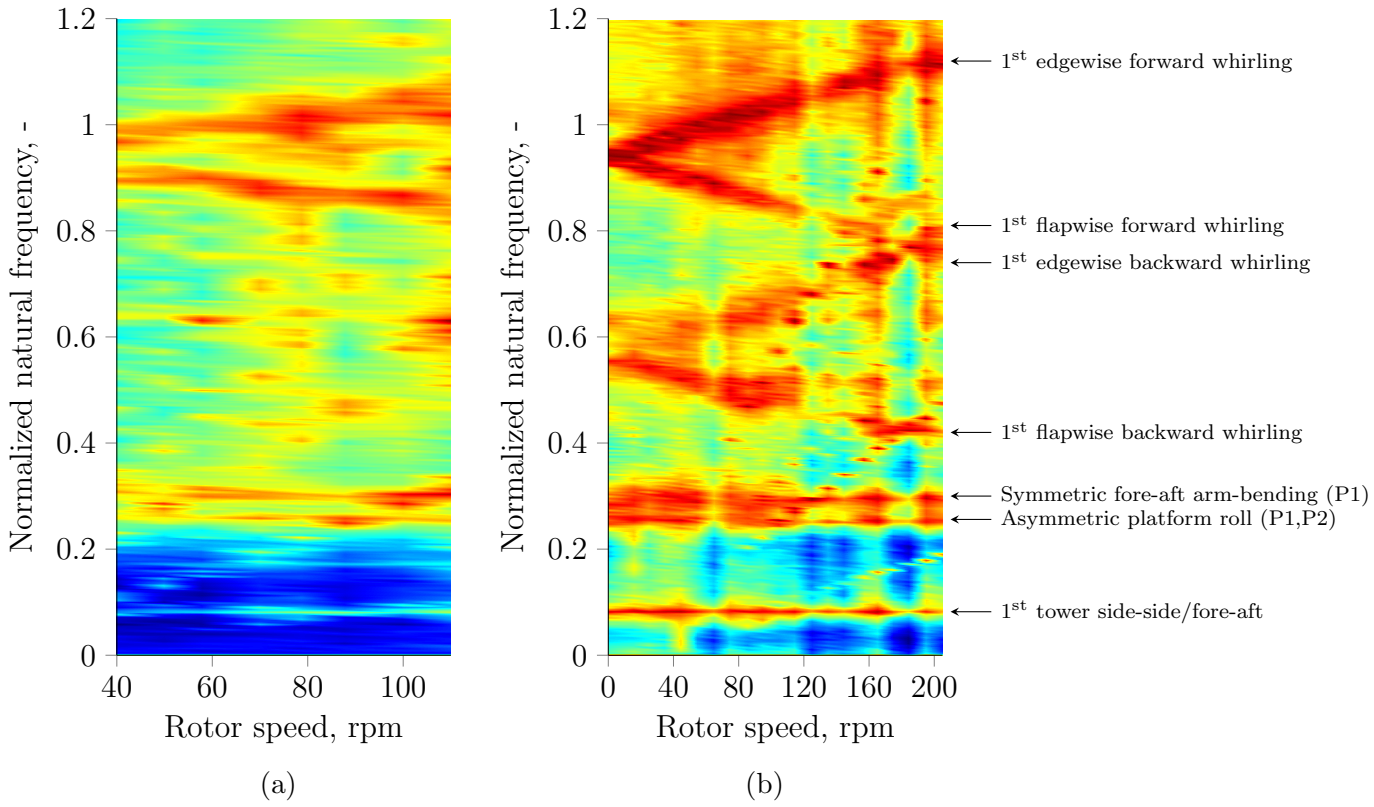

Figure 7. Campbell diagrams for the experimental setup based on the automated impulse mechanism from 40 to 110 rpm (a), and using the metal brushing technique from 0 rpm to 205 rpm (b). Both diagrams used acceleration data from rotor R02 in global z direction.

the numerical model where it is assumed fixed. In general, the metal brush technique yields a Campbell diagram with less noise. One of the reasons for this is that the impulse excitation strategy introduces periodic impulses into the system at multiples of the rotor speed. Increasing the rotor speed does not show any significant effect on the tower modes.

Campbell diagrams for the other accelerometers have been analyzed but are not shown in the paper. The Campbell diagram for the accelerometer on rotor R04 oriented in the global z-direction shows almost identical results as the once seen in Figure 7 (b). For the accelerometers on R02 and R04 the whiling splits are not as pronounced as for the rotors on P1 but the edgewise modes can be observed. For the accelerometers on the tower it is only possible to see whirling splits for the edgewise rotor modes.

4. Conclusion

A 1/30 scaled-down experimental setup simulated the dynamic behavior of the Vestas four-rotor demonstrator wind turbine in this paper. After scaling the blade tip height was reduced from 75 m to 2.5 m, and the rotor diameter from 27 m to 0.9 m. The scaling was performed by equal the Froude number for the experimental setup with the Vestas turbine to achieve comparable dynamic behavior. Numerical modeling of the experimental setup was performed in HAWC2 to compare mode shapes, and natural frequencies. In general, there was good agreement between the experimental setup and the Vestas turbine in terms of dynamic behavior, but difficulties were encountered in scaling the complex interface between tower, arm-structure, and yaw drive. This resulted in a stiffer setup at these connections points for the experimental setup compared

to the Vestas turbine which increased some of the natural frequencies. For the standstill case, a metal brush technique was used to excite natural frequencies. To find the relation between rotor speed and natural frequencies for the experimental setup, an automated impulse mechanism was proposed. The principle of the mechanism was to provide an impulse excitation to the blades as they passed a specific azimuth angle in the rotor plane. The testing was performed at equal rotor speeds. The output signal from accelerometers was effected by noise when using the automated impulse mechanism. Moreover, at around 110 rpm, the setup experienced large vibrations so it was not possible to continue increasing the rotor speed. To improve the results, the metal brushing technique was used for the rotating tests. This improved the results, and it was shown that the flapwise and edgewise whirling splits proportional to the rotor speed as can be observed for single-rotor wind turbines. This result confirmed analytical results reported in the other published research literature.

Acknowledgments

This work was support by Innovation Fund Denmark [grant 7038-00113A]; and Vestas Wind System A/S. Special thanks to Matiyas Tsegay Korsa, Johan Thoft Krogshave, Till Boettjer and Emily Rose Shereen Filsoof for her assistants on the experiments.

References

[1] Jamieson P. Innovation in Wind Turbine Design. Wiley Online Library; 2011.
[2] Skjoldan PF, Hansen MH. On the similarity of the Coleman and Lyapunov-Floquet transformations for modal analysis of bladed rotor structures. Journal of Sound and Vibration. 2009;327(3-5):424–439.
[3] Van der Veen G, Van Wingerden JW, Verhaegen M. Closed-loop system identification of wind turbines in the presence of periodic effects. In: Proc. of the 3rd conference, The Science of Making Torque from Wind; 2010. .
[4] Kim T, Larsen TJ, Yde A. Investigation of potential extreme load reduction for a two-bladed upwind turbine with partial pitch. Wind Energy. 2015;18(8):1403–1419.
[5] Hansen MH. Modal dynamics of structures with bladed isotropic rotors and its complexity for two-bladed rotors. Wind Energy Science. 2016;1(2):271–296.
[6] Riva R, Cacciola S, Bottasso CL. Periodic stability analysis of wind turbines operating in turbulent wind conditions. Wind Energy Science Discussions. 2016;p. 1–50.
[7] Filsoof OT, Hansen MH, Yde A, Zhang X. Dynamic Modeling and Stability Analysis of a Dual-Rotor Wind Turbine. In: ASME 2018 International Design Engineering Technical Conferences and Computers and Information in Engineering Conference; 2018. .
[8] Filsoof OT, Hansen MH, Yde A, Bøttcher P, Zhang X. Modal Dynamics of a Three-Bladed Tri-Rotor Wind Turbine. In: Advances in Engineering Materials, Structures and Systems: Innovations, Mechanics and Applications; 2019. .
[9] Filsoof OT, Yde A, Zhang X. Operational Modal Analysis of a Multi-Rotor Wind Turbine. In: The 29th International Ocean and Polar Engineering Conference. International Society of Offshore and Polar Engineers; 2019. .
[10] Larsen TJ, Kim T. Experimental and numerical study of Rotor dynamics of a two- and three-bladed wind turbine. International Journal of Offshore and Polar Engineering. 2016;26(4):355–361.
[11] Jain A, Robertson AN, Jonkman JM, Goupee AJ, Kimball RW, Swift AHP. Fast code verification of scaling laws for deepcwind floating wind system tests. Proceedings of the International Offshore and Polar Engineering Conference. 2012;(April):355–365.
[12] Tarpø M, Nabuco B, Skafte A, Kristoffersen J, Vestermark J, Amador S, et al. Operational modal analysis based prediction of actual stress in an offshore structural model. Procedia engineering. 2017;199:2262–2267.
[13] HAWC2 website;. Accessed: 2020-02-28. `http://hawc2.dk/`.
[14] Hansen MH. Aeroelastic instability problems for wind turbines. Wind Energy. 2007;10(6):551–577.